Nanoscale

PAPER

View Article Online
View Journal | View Issue

Cite this: *Nanoscale*, 2014, **6**, 931

High performance PbS quantum dot sensitized solar cells *via* electric field assisted *in situ* chemical deposition on modulated TiO_2 nanotube arrays†

Liang Tao,[a] Yan Xiong,[b] Hong Liu*[ab] and Wenzhong Shen*[ab]

Received 22nd August 2013
Accepted 15th October 2013

DOI: 10.1039/c3nr04461k

www.rsc.org/nanoscale

Quantum dot sensitized solar cells (QDSSCs) are attractive photovoltaic devices due to their simplicity and low material requirements. However, efforts to realize high efficiencies in QDSSCs have often been offset by complicated processes and expensive or toxic materials, significantly limiting their useful application. In this work, we have realized for the first time, high performance PbS QDSSCs based on TiO_2 nanotube arrays (NTAs) *via* an *in situ* chemical deposition method controlled by a low electric field. An efficiency, η, of ~3.41% under full sun illumination has been achieved, which is 133.6% higher than the best result previously reported for a simple system without doping or co-sensitizing, and comparable to systems with additional chemicals. Furthermore, a high open-circuit voltage (0.64 V), short-circuit current (8.48 mA cm^{-2}) and fill factor (0.63) have been achieved. A great increase in the quantity of the loaded quantum dots (QDs) in the NTAs was obtained from the *in situ* electric field assisted chemical bath deposition (EACBD) process, which was the most significant contributing factor with respect to the high J_{SC}. The high V_{OC} and FF have been attributed to a much shorter electron path, less structural and electronic defects, and lower recombination in the ordered TiO_2 NTAs produced by oscillating anodic voltage. Besides, the optimal film thickness (~4 μm) based on the NTAs was much thinner than that of the control cell based on nanoporous film (~30.0 μm). This investigation can hopefully offer an effective way of realizing high performance QDSSCs and QD growth/installation in other nanostructures as well.

Introduction

Quantum dots (QDs) have received tremendous attention due to their attractive optical and electronic properties,[1–3] and have been integrated into different opto-electronic devices, *e.g.*, quantum dot sensitized solar cells (QDSSCs).[4] Although the conversion efficiency of QDSSCs has still not caught up with those of dye-sensitized solar cells (DSSCs)[5] or quantum dot heterojunction solar cells,[6] their relatively lower material requirements still make them competitive subjects for further development. For instance, successful photovoltaic (PV) effects in QDSSCs have been reported using materials such as InP,[7] InAs,[8] CdS,[9–11] CdSe,[12] CdTe,[13] Ag_2S (ref. 14) and PbS.[15–17] Among these materials, PbS has emerged as a promising material due to its high light absorption coefficient[18,19] and easily adjustable energy gaps with a large exciton Bohr radius of 20 nm. Moreover, according to research on the multiple exciton generation (MEG) effect, the use of PbS is a suitable basis for the realization of the MEG effect, due to its narrow bandgap (E_g).[20] With a view to application, the features of PbS QDs such as their non-toxicity throughout the fabrication process and their ease of accessibility, endow this material with a huge potential for mass production.

Generally, there are two routes to improve the performance of sensitized solar cells based on QDs: (1) morphological and nanostructural modification of the photosensitive and substrate materials; (2) componential modification of the photosensitive and substrate materials with chemical doping or the addition of other chemical compounds. In an example of the first route, the Grätzel research group took the lead making a PbS QDDSC of measurable efficiency using a TiO_2 nanoporous electrode.[21] Initially achieving a conversion efficiency of 0.49% under 0.1 sun, the efficiency of this cell was enhanced to 1.46% by the same group using comprehensive methods.[22] The second route, which has drawn more attention in previous studies, has resulted in more significant advantages in recent years. By means of co-sensitization, an efficiency of the fabricated cells of 2.21% was achieved (with CdS coating layer)[23] and >4.0% (with CdS QDs).[24] By means of material doping, an efficiency of 2.01% has been reached with Cu (ref. 25) and 5.6% with Hg (ref. 26,27)

[a]*Laboratory of Condensed Matter Spectroscopy and Opto-Electronic Physics, Key Laboratory of Artificial Structures and Quantum Control (Ministry of Education), Department of Physics, Shanghai Jiao Tong University, 800 Dong Chuan Road, Shanghai, 200240, People's Republic of China. E-mail: liuhong@sjtu.edu.cn; Fax: +86 (0)21 54743243; Tel: +86 (0)21 54743243*

[b]*Institute of Solar Energy, Department of Physics, Shanghai Jiao Tong University, 800 Dong Chuan Road, Shanghai, 200240, People's Republic of China. E-mail: wzshen@sjtu.edu.cn; Fax: +86 (0)21 54747552; Tel: +86 (0)21 54747552*

† Electronic supplementary information (ESI) available: Fig. 1S to 4S and Tables 1S to 2S. See DOI: 10.1039/c3nr04461k

(the records were 3.6% for PbS/TiO_2 (ref. 28) and 4.0% for PbS/PbSe (ref. 29) in heterojunction solar cells). Recently, through a combined structural and chemical development from the QDSSC concept, *e.g.*, perovskite-sensitized solar cells, a remarkable efficiency of 15.0% has been achieved for a $CH_3NH_3PbI_3$ system.[30]

However, despite these significant achievements of higher cell efficiencies, they have often been at the expense of complex fabrication methods or the necessity of toxic materials. Therefore we have turned our attention to seeking cheaper and simpler methods. Until now, the most typical investigations on QDSSCs incorporating PbS have been carried out on porous nanocrystalline TiO_2 layers by a soaking process. However, this classical cell style has led to significant problems in key processes such as carrier transport and the effective loading of sensitizers. These problems can be much more serious for QDs, which are normally larger than dye molecules and also exhibit poorer contact with the substrate. Moreover, the random connections in the porous film can also influence the carrier transport in the substrate.

With respect to electron transport in the substrate, oriented anodic TiO_2 nanotube arrays (NTAs) have offered an alternative to porous films for use in DSSCs.[31,32] In terms of QDSSCs, some reports have indicated that the vertical geometry of the NTAs appeared to be more suitable than the conventional random pore network for the fabrication of solid-state cells utilizing polymeric sensitizer materials.[33,34] Studies on DSSCs have also shown that NTA-based cells normally require a lower thickness to achieve the same efficiency,[35] which indirectly proves the faster transport of electrons in the straight tube structure. Moreover, anodic NTAs are uniformly organized and easy to control and modify. However, some difficulty has been met when attempting to utilize NTAs in QDSSCs with a view to achieving high conversion efficiencies. One key problem is that most anodic NTAs have not demonstrated as good electron transport properties as expected when incorporated into practical devices.[36,37]

More importantly, another key problem is the loading of sensitizers onto the substrate, which can influence both the photo-carrier generation and the transport in the sensitizer/substrate interface. The shortage of deposition quantity was partly resolved with the use of certain fabrication processes, such as the successive ionic layer adsorption and reaction (SILAR) method.[23,24] Nevertheless, the size of the sensitizers has still remained an essential limiting factor for them to enter deep into the substrate, which has an adverse effect on the effort to increase the effective surface area of the substrate. The chemical bath deposition (CBD) method has helped to resolve this problem, in which QDs are formed directly on the substrate by ionic species from precursor solutions. However, most CBD experiments for QD fabrication require high temperatures for the reactions to be successful.[38] Considering the ionic reaction mechanism of these systems, more effective methods for the QD loading process would be possible based on a combination of CBD and the application of an electric field. Consequently, the key point to solving this problem in a simple way, would lie in the simultaneous design of new innovative TiO_2 nanostructures with reliable transport pathways, and a suitable QDs loading method for effective light capture.

In this work, we have successfully realized high performance PbS QDSSCs based on TiO_2 NTAs for the first time, by means of a novel and effective QDs growth method aided by physical modulation of the NTAs. QDs have been directly manufactured inside ordered TiO_2 NTAs with the application of a low cathodic bias. Using this method, it is possible to achieve an increase of sensitizer loading, the restriction of recombination and the improvement of carrier transport at the same time. NTAs fabricated using oscillating anodic voltages have been applied as substrates with better ordering and enhanced carrier transport abilities.[37] Finally, the presented QDSSC has finally achieved a conversion efficiency of 3.41% under AM1.5, which is 133.6% higher than the previous maximum record (1.46%), with no chemical doping or co-sensitizing,[22] which is comparable to those records for cells with additional chemical involvement or in heterojunction cells.[23,24,28,29] The field strength and surface modification[39] of the NTAs have been explored in order to increase the surface area available for adsorption. Other parameters such as the bandgap of PbS QDs, the thickness of the NTA film, and the amplitude of the modulated voltage have also been investigated to identify the suitable initial conditions. For comparison, samples with *ex situ* QD loading by direct soaking were also investigated under the above conditions. In general, a new and simple way to promote anodic NTAs to be a very suitable substrate with high sensitizer adsorption and carrier transport ability, has been established and studied. Notably, high performance QDSSCs based on NTAs have been achieved for the first time. Finally, the electric-field-assisted *in situ* chemical deposition used in this experiment has been proved as an effective tool for the growth of quantum dots inside tubular structures.

Experimental section

Fabrication and modification of porous films and TiO_2 NTAs

The nanoporous TiO_2 films were fabricated from TiO_2 powder (Degussa P25). 2.4 g P25 powder was mixed with 0.75 g ethyl cellulose (46 cp, Sigma-Aldrich) in 9 ml terpineol (99.5% purity, Sigma-Aldrich), coated onto the FTO substrate and then annealed at 500 °C for 1 h in air. The Ti sheets (0.25 mm thick, 99.7% purity, Sigma-Aldrich) were cleaned with methanol, ethyl alcohol, acetone, and isopropyl alcohol in sequence in an ultrasonic bath to remove any impurities. Highly ordered TiO_2 NTAs were prepared by a second anodization of the Ti sheet in a two-electrode cell. The first anodization was performed at 5 °C in a solution of 0.5 wt% of NH_4F and 2.0 wt% of H_2O in ethylene glycol (E.G.). The growth time depends on the oxidation voltage and the expected film thickness. The second anodization was performed at constant voltage or modulated voltage at 5 °C in the same solution. All of the nanoporous films and NTAs were treated with 0.3% HF for 30 min and 0.2 M $TiCl_4$ before the installation of the QDs. The treated samples were then rinsed with deionized water and ethanol, followed by annealing in air at 500 °C for 1 h at a heating rate of 2 °C per min.

Ex and *in situ* growth of PbS QDs

In the *ex situ* QD loading by direct soaking, the QDs were prepared by the reaction of two precursors. The lead oleate was prepared by dissolving PbO in oleic acid (OA) at different concentrations (molar ratio of PbO and OA ranged from 1 : 2 to 1 : 16) at 120 °C under an Ar atmosphere for 1 h. Then a solution of bis(trimethylsilyl)sulfide (TMS) in octadecene (ODE) was injected into the stirring lead oleate solution at 120 °C. The molar ratio of S and Pb was kept at 1 : 2, while the amount of ODE was varied so that the total mixture volume was the same. Smaller particle sizes were obtained when the amount of OA was reduced by diluting with ODE. The PbS QDs were stored in toluene under an Ar atmosphere.

For the *in situ* growth of QDs on the substrate with electric-field-assistance, the experiment was carried out in a sealed and oxygen-free container with electrodes (detailed setup is described by Fig. 4S in the ESI†). Two precursor solutions with much lower concentrations (molar ratio of PbO, TMS, OA and ODE was 2 : 1 : 80 : 240) were mixed and introduced into the container. The initial temperature of the precursors was 120 °C. The mixed solution was then kept at room temperature for 24 h. The substrate was fixed in the container, with different bias voltages from 0 V to −5 V (detailed illustration of the device can be found in Fig. 4S in the ESI†). The bias was set to negative to prevent possible damage of the TiO_2 substrate and to ensure an excess of Pb^{2+} cations.

Fabrication of QDSSCs

The effective area of all of the TiO_2 NTA films for solar cells was 0.25 cm^2, which is the typical size in related research. In the soaking process, the samples were immersed in PbS QDs toluene solution for 24 h under an Ar atmosphere. For the *in situ* growth process, the annealed Ti sheet was used as the low potential electrode as well. After sensitizing, these films were mounted together with a counter electrode with a platinum black (prepared by coating FTO glass with a 0.004 M H_2PtCl_6 solution in ethanol and then heating in air at 200 °C for 1 h) to form the QDSSCs. The liquid electrolyte was injected into the cells with a syringe, which consisted of 0.1 M iodine (I_2), 0.1 M lithium iodide (LiI), 0.6 M tetra-butylammonium iodide, and 0.5 M 4-*tert*-butyl pyridine in acetonitrile (CH_3CN, 99.9%).

Characterization of the materials and devices

The morphology and distribution of the PbS QDs were characterized by field emission transmission electron microscopy (TEM, JEM-2100F, JEOL USA Inc.). The same technique was also employed to investigate the detailed structural information of the TiO_2 NTA materials. The surface morphology of samples was characterized by field emission scanning electron microscopy (FE-SEM, JEOL JSM). The elemental analysis was performed by energy dispersive X-ray (EDX) during the FE-SEM observation. Detailed microstructures were investigated by selected area electron diffraction (SAED) during the high-resolution (HR)-TEM measurements. Absorption spectra were recorded by Fourier transform infrared spectroscopy (FTIR, Nexus870, Nicolet) and Ultraviolet Spectroscopy (UV, THR1000, Jobin Yvon). The photocurrent density–photovoltage (*J*–*V*) characteristics of the QDSSCs were measured under AM1.5 (100 mW cm^{-2}) illumination provided by a solar simulator (Oriel Sol 2A) with a Keithley 2400 source meter.

Results and discussion

Nanoporous films, as shown in Fig. 1a and b, have long been a focus for particle loading and have shown good efficiency in solar cells. Therefore it was chosen for the control sample for the whole experiment. As is well known for this kind of structure, photogenerated electrons need to pass through a tortuous and complex path, as also shown by Fig. 1a. PbS QDs of various sizes (central size ranging from 3 nm to 12 nm, details can be found in Fig. 1S in the ESI†) were synthesized according to the method reported by Hines *et al.*[40] for the fabrication of QDSSCs. Afterwards, the absorption spectra of the TiO_2 porous film and the PbS QDs toluene solution were measured to further characterize the as-fabricated QDs. For the TiO_2 substrate, the absorption edge appears at ~390 nm corresponding to the 3.2 eV E_g; for the PbS QDs, corresponding to four scales of particle sizes, the location of the absorption valley ranges from 744 nm, 1086 nm, 1344 nm to 1754 nm, covering the most valuable portion of the visible and infrared light spectrum.

The relevant energy levels of the PbS QDs in Fig. 1d are taken from the results of cyclic voltammetry (CV) measurements from

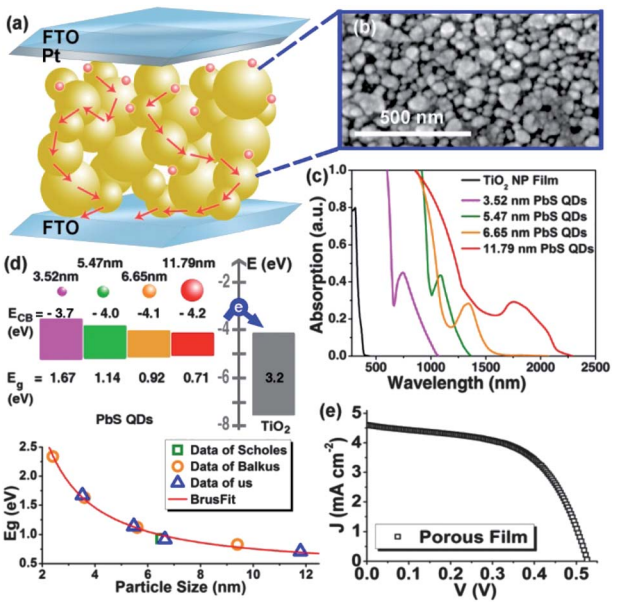

Fig. 1 Control cell with porous substrate: (a) schematic illustration of the cell structure with the porous film and the electron transport pathway (arrows) from the top TiO_2 film to the bottom FTO; (b) top view SEM image of the TiO_2 porous film grown from Degussa P25; (c) absorption spectra of the TiO_2 porous film and the PbS QDs toluene solution; (d) energy band diagram of the PbS QDs and the TiO_2 substrate (top), and the relationship between QDs particle size and bandgap E_g (bottom); (f) *J*–*V* characteristics of the PbS QDSSC on the porous TiO_2 layer.

the paper of Hyun's group.[41] According to the Brus theory, the bandgap (E_g) of the QDs depends on the band gap of the bulk material, the quantum size effect (QDs radius, R), and the Coulomb effect.[42] We calculate the bandgap from the equation:

$$E_g = E_{g0} + h^2(1/m_n^* + 1/m_p^*)/8R^2 - 1.78e^2/\varepsilon R,$$

where E_{g0} and ε are the band gap and the dielectric constant of the bulk materials, respectively, $m_{n,p}^*$ are the effective masses of the electron and hole, respectively, and e is the electron charge. Calculated values are given in Fig. 1d, which shows the energy band diagram and the relationship information between the particle size and the energy bandgap of the PbS QDs. Comparing the Brus theory with the result from our PbS QDs used in this work and in that of other research groups,[16,40] it is clear that the absorption bands of PbS QDs can be easily tuned from narrow to wide bandgap by controlling the particle size. After decoration of the TiO_2 nanotubes with PbS QDs ($E_g = 1.14$ eV), the cell offered a conversion efficiency (η) of 1.38%, with J_{SC} = 4.60 mA cm^{-2}, V_{OC} = 0.53 V, FF = 0.57 (see Fig. 1e), and thickness = 30 μm. This result is just a little lower than the previous record,[22] which offers a good basis for comparisons of PbS QDSSCs on NTAs.

Nevertheless, 1.38% is still a low value, which is strongly influenced by the significant probability of the electrons to change their direction during transport in the porous substrate. Therefore, TiO_2 NTAs were chosen as the substrate for further investigation in this experiment, which were simply prepared by a second anodization of the Ti sheet. Their electron pathway (normally considered to be straighter than that of a porous film) and the corresponding SEM image are shown in Fig. 2a and b. Notably, certain defects around the surface would induce some relative resistive effects in the electron pathway. The corresponding HR-TEM image in Fig. 2c demonstrates that PbS QDs (tiny black spots) exist in the tubes, which indicates the successful incorporation of QDs into the TiO_2 NTAs. Sensitized by four different sizes of QDs respectively, the corresponding η of the QDSSCs were 0.32%, 0.65%, 0.41%, and 0.17% (J–V curves can be found in Fig. 2d). The different efficiencies can be attributed to two factors: (1) the light absorption ability of the QDs due to quantum size effect; (2) the loading ability of the QDs into the tubes influenced by the particle size. It can be observed that the QDs with the size 5.47 nm (E_g = 1.14 eV) showed relatively optimal behaviour after being loaded in QDSSCs.

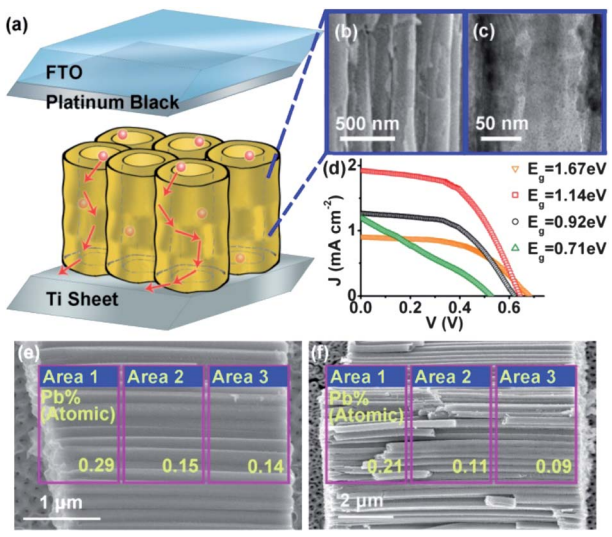

Fig. 2 QDSSCs with normal NTAs: (a) schematic illustration of the cell structure with normal TiO_2 NTAs and the transport pathway (arrows) from the top TiO_2 film to the bottom Ti sheet; (b) lateral view SEM image of normal TiO_2 NTAs; (c) HR-TEM image of nanotubes filled with PbS QDs. Charac-333withic.3(i)-9.HR-T53d.l-239.sTD(5been)-31y f6.5(about)16.1(u)0(s)T/F11Tf163980TD0Tj/FTj/F8g celb81gaph-218.5.91680Troofavera

However, it can be seen that even the optimal efficiency in the PbS QDSSCs with normal TiO_2 NTAs is significantly lower than that with porous TiO_2 substrates. The lower efficiency can be caused by the unfavourable QDs absorption and the morphological defects. As can be seen in Fig. 2e and f, the average Pb concentration in the long tubes is significantly lower than that in the short ones, revealing the remarkable impact of film thickness on the loading efficiency. With respect to the defects, multiple scattering would take place for each electron during the transport process owing to the surface discontinuity.[43] Furthermore, certain trapping effects can also arise due to the presence of oxygen defects in the anodic NTAs, according to the research from Schmuttenmaer's research group.[36] Therefore, the key to solving the low η problem is to increase the absorption and improve the tube quality. According to our recent research, simple physical and chemical modulation can contribute greatly to meeting the desired efficiencies similar to those of DSSCs,[34] thus we carried out a series of experiments on NTAs with different layer thicknesses using a periodically modulated voltage (related information can be found in Fig. 3S in the ESI†) and controlled mechanical stirring with in the presence of HF. Fig. 3a shows the schematic illustration of the cell with TiO_2 NTAs prepared by the phys-chem modulation, with the corresponding morphology shown by Fig. 3b and c. It can be clearly seen that more straight tubes have been formed with secondary structures and fewer defects, which allowed higher electron transport, better absorption of QDs, and a lower probability of recombination.

As a result, the relationship between the film thickness, the corresponding cell efficiency (with PbS QDs of E_g = 1.14 eV chosen as the sensitizer), and the growth time is demonstrated in Fig. 3d. It was observed that the efficiency reached the maximum (~1.40%) at the thickness of ~5.4 μm (corresponding growth time of 300 s). In DSSCs, the optimum thickness of TiO_2 NTAs was generally reported to be about 20 μm,[44] which is still much thicker than the 5.4 μm in the present PbS QDSSCs. Fig. 3e–j show the further investigation of modulated NTAs with different oscillation voltages, from 180 ± 0 V to 180 ± 10 V. All of the images were taken at the same height of the tubes. The inner diameter became larger while the outer diameter remained about the same. As shown in Fig. 3k, a maximum efficiency (η) of about 1.62% was achieved at 180 ± 5 V with J_{SC} = 4.63 mA cm^{-2}, V_{OC} = 0.64 V, and FF = 0.55, which is

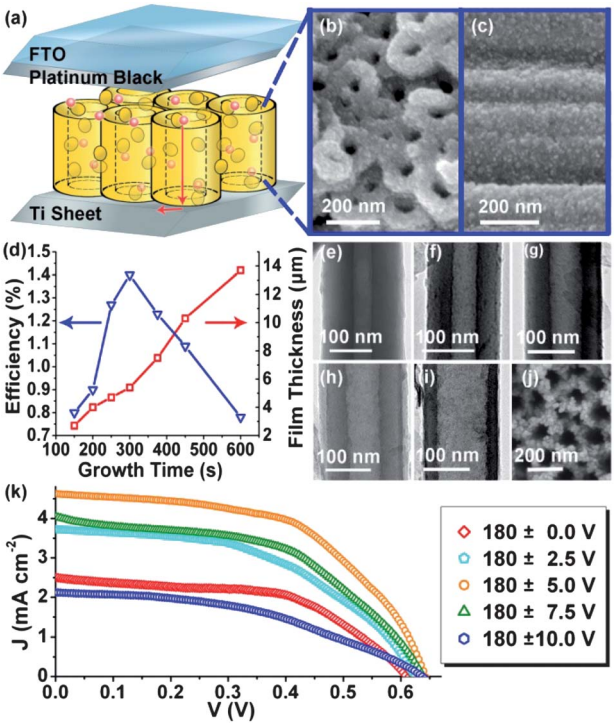

Fig. 3 NTAs modulated by oscillating voltage and chemical treatment, and the corresponding cell characteristics: (a) schematic illustration of the cell structure with modulated TiO_2 NTAs and the electro-pathway (arrows) from the top TiO_2 film to the bottom Ti sheet; (b and c) NTAs by 180 ± 5 V; (d) film thickness and corresponding cell efficiency *versus* growth time of the modulated TiO_2 NTAs photoanode; (e–i) lateral view TEM image of modulated TiO_2 NTAs with different oscillation voltages, from ±0 V to ±10 V; (j) top view SEM image of modulated TiO_2 NTAs with 180 ± 5 V for 300 s; (k) *J–V* characteristics of our solar cells under different oscillation voltages.

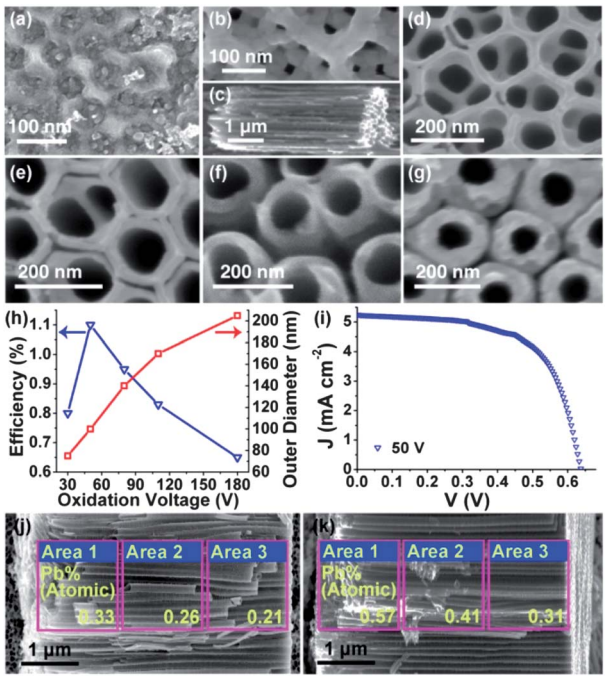

Fig. 4 Optimization of NTA size: (a–g) SEM images of TiO_2 NTAs under different oxidation voltages from 10 V to 180 V: (a) 10 V, (b) 30 V, (c) 30 V, lateral view, (d) 50 V, (e) 80 V, (f) 110 V, (g) 180 V; (h) outer diameter of the modulated TiO_2 NTAs and corresponding cell efficiency *versus* oxidation voltage; (i) the *J–V* characteristic of the optimal condition (anodization voltage 50 V) with $\eta = 2.08\%$ and thickness = 4.4 μm; (j and k) the Pb concentration in different selected areas of TiO_2 NTAs after soaking PbS QDs: (j) without and (k) with voltage modulation (50 ± 1.4 V).

significantly higher than the corresponding results of the porous substrate.

Though the efficiency of NTA-based PbS QDSSCs has reached a new record in comparison to previous results, it is still quite low compared to the highest value of QDSSCs in general, *i.e.*, 4.92% for a CdS/CdSe co-sensitized solar cell.[12] According to calculations based on a hexagonal close packed model, the area available for adsorption increases rapidly as the diameter decreases under the same tube spacing and arrangement. For example, the TiO_2 NTAs fabricated under a high electric field with a large outer diameter (such as 210 nm) have an absorbable area of 8.23 $cm^2\ \mu m^{-1}$, while those tubes fabricated under a low field with a small outer diameter (such as 70 nm) have an absorbable area of 22.21 $cm^2\ \mu m^{-1}$. To study the influence of the NTA diameter on the cell efficiency, a series of TiO_2 NTAs were simply fabricated without any treatment, as shown in Fig. 4a–g. They had identical lengths (~5 μm), wall to diameter ratio (1 : 5) and tube spacing (10 nm), while their diameters ranged from 75 nm to 205 nm. As can be seen from Fig. 4a, too low an anodic voltage led to the formation of a porous structure in this case. This limited the smallest obtainable diameter to 75 nm (at 30 V as shown in Fig. 4b and c) where a tubular structure could be formed.

Afterwards, those tubes were installed into QDSSCs. The relationship of outer diameter, corresponding cell efficiency, and oxidation voltage is revealed in Fig. 4h. Within the probed values, the optimum voltage is 50 V, where the cell had a maximum efficiency of 1.10% without any treatments (therefore we chose 50 V as the standard voltage in the following experiments). The result under a higher field (50–180 V) show that η was reduced along with a decrease of the absorbable area, consistent with our expectations. A series of tubes with different thicknesses were then assembled into cells adding physical modulation (details can be found in Table 1S in ESI†). The corresponding *J–V* curve is shown in Fig. 4i, and the optimal η of 2.08% can be obtained, where the η was 50.7% higher and the film thickness was 18.5% less in comparison to the previous results with 180 V through the same treatment as shown in Fig. 3g. The lower requirement of NTA thickness results in significant advantages in terms of cost and stability for possible future mass production and practical application. To elucidate the contribution of the loading ability of the sensitizers in this experiment, we have further investigated the adsorption of PbS QDs in TiO_2 NTAs. EDX measurements shown in Fig. 4j and k clearly show that the absorption of PbS QDs was significantly higher in smaller tubes than in the larger diameter tubes shown in Fig. 2e.

Despite the increase of the QD loading shown in Fig. 3g, 4h and i, these experiments have all been performed with *ex situ* treatment by direct soaking of NTAs in QD dispersions. Though the size of the QDs (normally below 10 nm) is much lower than the inner diameter of the tubes, possible clustering of QDs may still take place, preventing further loading into deeper positions within the tubes. Therefore we turned to the direct growth of QDs on the inner surfaces of the NTAs, in which ions instead of QDs will be the entities entering the tubes. The normal CBD method in nanostructures often requires high temperatures (normally >50 °C).[45,46] Since the reactants were mostly ionic species, we tried to apply an external outer electric field to the TiO_2 anodes to encourage the dispersion of more ions onto the entire effective surface of the tubes and accelerate the reaction. We call this method "electric-field assisted chemical bath deposition" (EACBD) due to this difference from the conventional CBD method. It has been found by many groups that at high temperature, the nucleation has been completed as soon as the precursors come into contact with each other.[47,48] Therefore the experiment was carried out at room temperature. Pt was used as the counter electrode, and two heated precursor solutions were blended in a container under an Ar atmosphere (more detailed information can be found in Fig. 4S in the ESI†). The concentration of precursor solutions was controlled at a low level to avoid reactions proceeding too quickly before the ions had adsorbed onto the surface of the TiO_2 tubes. The TiO_2 NTAs were negatively biased in order to prevent possible damage to the TiO_2 NTAs due to anodization.

Fig. 5a–f are the corresponding TEM images showing the morphologies and absorption situations of the PbS QDs at different positions of the TiO_2 NTAs. Apparently, a large quantity of as-formed PbS QDs was formed at the tube surface. However, the QDs formed by the EACBD method seemed to have significant size distribution depending upon their depths within the tubes. As illustrated by the HR-TEM images in Fig. 5b, d and f, the QDs had a larger average size (~6 nm) at the top and a smaller size at the bottom (~2.5 nm). This is understandable if considering the concentration gradient of the reaction species due to diffusion processes inside the NTAs, which can significantly influence the core growth of the QDs. To quantitatively describe the loading efficiency, the Pb distribution was examined by EDX (Fig. 5h). The results show that the overall Pb concentration was significantly higher than the result obtained from *ex situ* fabrication (shown by Fig. 2 and 4). Moreover, the distribution of the Pb QDs was also more homogeneous than that in the *ex situ* soaking experiment. The as-fabricated samples were installed into QDSSCs and their corresponding *J–V* characteristics displayed in Fig. 5d. The corresponding *J–V* characteristic is indicated in the blue curve of Fig. 5g. An efficiency η of ~3.15% has been achieved, together with $J_{SC} = 7.69$ mA cm^{-2}, $V_{OC} = 0.65$ V, FF = 0.63 and film thickness = 4.4 μm. This enhancement of efficiency was a result of the higher fill factor, while the J_{SC} and V_{OC} are almost the same.

As shown by this experiment, driven by the electric field, higher yields of QDs can be achieved at the low potential electrode at low temperature, compared to conventional thermo chemical processes. To investigate the effect of different field

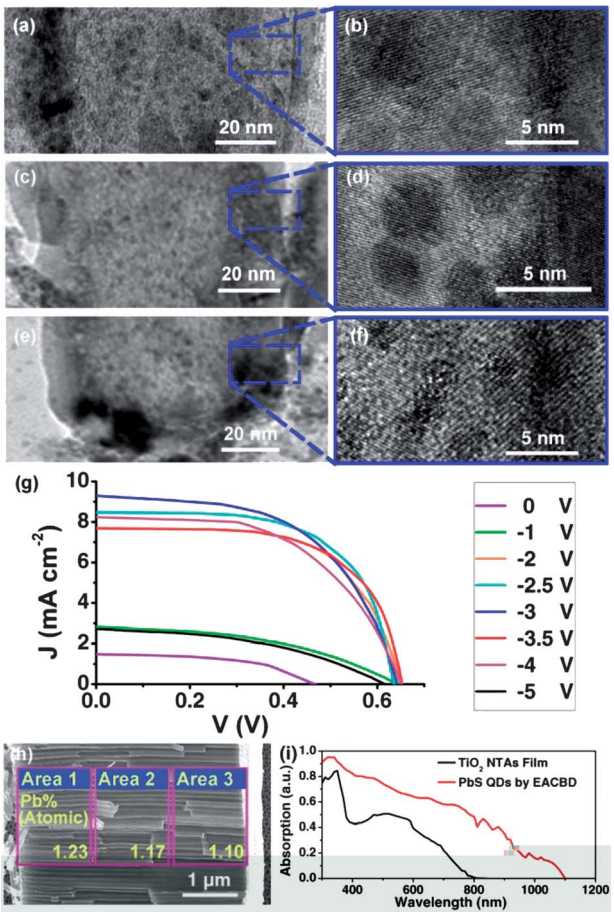

Fig. 5 *In situ* EACBD growth of QDs in NTAs and the corresponding cell performance: (a–f) TEM images of PbS QDs loaded TiO_2 NTAs (anodization voltage: 50 ± 1.4 V, bias voltage during growth: −2 V) at different positions in a tube: (a and b) top; (c and d) middle; (e and f) bottom. (g) *J–V* characteristics of our solar cells after the modulation and *in situ* growth under different applied voltages. (h) The corresponding Pb concentration in different positions of TiO_2 NTAs. (i) Absorption spectra of EACBD sample with the maximum efficiency.

intensities, further experiments were carried out under various voltages from 0 (which corresponds to a pure CBD experiment without an applied electric field) to −5 V. When no voltage was applied, an efficiency of only 0.36% was achieved. As the modulus of the voltage was increased, the conversion efficiency first increased, reaching a maximum of 3.41% at −2.5 V, and then decreased again at higher voltages (*e.g.*, η was only 0.72% at −5 V; detailed *J–V* characteristics at different stages are summarized in Table 2S in the ESI†). Compared to the control sample fabricated from a porous substrate and the soaking method, the efficiency and short-circuit current were improved by 147.1% and 84.3%, respectively. The relatively low efficiency at zero or low voltages can be explained by low PbS production under these conditions. When the electric field was increased, more Pb^{2+} could reach the inner surface of the TiO_2 tubes and therefore more PbS could form. However, when the field intensity in the reaction pool was too high (<−2.5 V), the reaction was accelerated so that PbS could form even at the top of

Table 1 Photovoltaic characteristic information of the PbS QDSSCs at different stages

Construction and method	Film thickness (μm)	η (%)	J_{SC} (mA)	V_{OC} (V)	FF
Porous film soaking	30	1.38	4.60	0.53	0.57
180 V NTAs soaking	5.3	0.65	1.92	0.64	0.53
50 V NTAs soaking	4.3	1.10	2.88	0.64	0.60
180 ± 5 V NTAs, soaking	5.4	1.62	4.63	0.64	0.55
50 ± 1.4 V NTAs, soaking	4.4	2.08	5.25	0.64	0.62
50 ± 1.4 V NTAs, EACBD: −2 V	4.4	3.15	7.69	0.65	0.63
50 ± 1.4 V NTAs, EACBD: −2.5 V	4.2	3.41	8.48	0.64	0.63

the tubes, which would inhibit the formation of PbS inside the tubes and reduce the final conversion efficiency of the cells.

We have clearly demonstrated that the *in situ* grown QDs by EACBD can easily achieve significantly higher efficiencies just by virtue of the PbS QDs, in comparison to the control samples with optimized *ex situ* loading on both porous and tubular substrates. To further correlate the changes in current density and voltage with the EACBD process, the absorption spectra of the highest η sample and the TiO_2 NTAs substrate were measured. The results shown in Fig. 5i show no significant absorption peak like the absorption peaks of the QDs shown in Fig. 1. Instead, compared to the absorption spectrum of the NTAs substrate, a significant increase of absorption has taken place in a wide range of wavelengths from 300–1100 nm. This broad absorption is likely attributed to the size variation shown by TEM images in Fig. 5e and f, which has consequently resulted in a higher conversion efficiency compared to the cells fabricated from the *ex situ* fabricated QDs with a single average size. The QD growth and size variation were realized by the one-step growth *via* chemical deposition under an applied electric field. Therefore, more generally the EACBD method we have applied here has shown its efficiency in improving the formation of materials which can be fabricated *via* ionic reactions from two precursors. It can be further improved by simple optimization of the reactant concentrations, or be alternated by changing the polarity of the electric field to adapted it to other reaction systems.

Conclusions

In this work, we have fabricated PbS QDSSCs based on TiO_2 NTAs for the first time, achieving the highest efficiency of 3.41% with an innovative *in situ* growth process and some simple treatments, 133.6% higher than the previously reported record on a porous photoanode which was fabricated by more complicated and expensive methods. The size of those well dispersed QDs can be in the range of 3 nm to 12 nm, while the optimal central size for use in a solar cell was found to be 5.47 nm, with $E_g \sim 1.14$ eV. The best cell had a short-circuit current density of 8.48 mA cm^{-2} and a high open-circuit voltage of 0.64 V with a fill factor of 0.63, benefiting from the carrier transport ability of the modulated NTAs and more importantly the high sensitizer loading efficiency resulting from the EACBD method. The optimized efficiency (3.41%) is significantly higher than the previous record with no introduction of new chemicals,[22] and is also comparable with those higher records with the involvement of chemical doping or co-sensitizing.[24–29] This *in situ* growth method can effectively promote TiO_2 NTAs as excellent substrates for high efficiency QDSSCs by significantly negating their shortcomings. For a clearer comparison, the key cell characteristics are illustrated in Table 1. In general, this work might have introduced an effective route for not only the improvement of the present QDSSCs, but also in the future developments and considerable latent advances in other similar structures and devices.

Acknowledgements

This work was supported by National Major Basic Research Project (2012CB934302), and Natural Science Foundation of China (11074169, 11174202, 11204176 and 61234005).

Notes and references

1 I. Robel, M. Kuno and P. V. Kamat, *J. Am. Chem. Soc.*, 2007, **129**, 4136–4137.
2 I. Moreels, K. Lambert, D. De Muynck, F. Vanhaecke, D. Poelman, J. C. Martins, G. Allan and Z. Hens, *Chem. Mater.*, 2007, **19**, 6101–6106.
3 X. Y. Yu, J. Y. Liao, K. Q. Qiu, D. B. Kuang and C. Y. Su, *ACS Nano*, 2011, **5**, 9494–9500.
4 N. Guijarro, T. Lana-Villarreal, Q. Shen, T. Toyoda and R. Gomez, *J. Phys. Chem. C*, 2010, **114**, 21928–21937.
5 A. Yella, H. W. Lee, H. N. Tsao, C. Yi, A. K. Chandiran, M. K. Nazeeruddin, E. W. G. Diau, C. Y. Yeh, S. M. Zakeeruddin and M. Grätzel, *Science*, 2011, **334**, 629–634.
6 L. Etgar, W. Zhang, S. Gabriel, S. G. Hickey, M. K. Nazeeruddin, A. Eychmuller, B. Liu and M. Gratzel, *Adv. Mater.*, 2012, **24**, 2202–2206.
7 T. Y. Zeng, E. Gladwin and R. O. Claus, *New Applications for Wide-Bandgap Semiconductors*, 2003, vol. 764, pp. 171–175.
8 P. R. Yu, K. Zhu, A. G. Norman, S. Ferrere, A. J. Frank and A. J. Nozik, *J. Phys. Chem. B*, 2006, **110**, 25451–25454.
9 W. T. Sun, Y. Yu, H. Y. Pan, X. F. Gao, Q. Chen and L. M. Peng, *J. Am. Chem. Soc.*, 2008, **130**, 1124–1125.
10 Y. L. Lee and Y. S. Lo, *Adv. Funct. Mater.*, 2009, **19**, 604–609.
11 H. Han, P. Sudhagar, T. Song, Y. Jeon, I. Mora-Sero, F. Fabregat-Santiago, J. Bisquert, Y. S. Kang and U. Paik, *Chem. Commun.*, 2013, **49**, 2810–2812.

12 Q. X. Zhang, X. Z. Guo, X. M. Huang, S. Q. Huang, D. M. Li, Y. H. Luo, Q. Shen, T. Toyoda and Q. B. Meng, *Phys. Chem. Chem. Phys.*, 2011, **13**, 4659–4667.
13 X. F. Gao, H. B. Li, W. T. Sun, Q. Chen, F. Q. Tang and L. M. Peng, *J. Phys. Chem. C*, 2009, **113**, 7531–7535.
14 G. Q. Ji, Z. Q. Liu, D. B. Guan and Y. T. Yang, *Appl. Surf. Sci.*, 2013, **282**, 695–699.
15 Y. Jin-nouchi, T. Hattori, Y. Sumida, M. Fujishima and H. Tada, *ChemPhysChem*, 2010, **11**, 3592–3595.
16 C. Ratanatawanate, C. R. Xiong and K. J. Balkus, *ACS Nano*, 2008, **2**, 1682–1688.
17 Q. Kang, S. H. Liu, L. X. Yang, Q. Y. Cai and C. A. Grimes, *ACS Appl. Mater. Interfaces*, 2011, **3**, 746–749.
18 I. Moreels, K. Lambert, D. Smeets, D. De Muynck, T. Nollet, J. C. Martins, F. Vanhaecke, A. Vantomme, C. Delerue, G. Allan and Z. Hens, *ACS Nano*, 2009, **3**, 3023–3030.
19 L. M. Peter, *J. Phys. Chem. Lett.*, 2011, **2**, 1861–1867.
20 Y. Yang, W. Rodriguez-Cordoba and T. Q. Lian, *Nano Lett.*, 2012, **12**, 4235–4241.
21 R. Plass, S. Pelet, J. Krueger, M. Gratzel and U. Bach, *J. Phys. Chem. B*, 2002, **106**, 7578–7580.
22 H. Lee, H. C. Leventis, S. J. Moon, P. Chen, S. Ito, S. A. Haque, T. Torres, F. Nüesch, T. Geiger, S. M. Zakeeruddin, M. Grätzel and M. K. Nazeeruddin, *Adv. Funct. Mater.*, 2009, **19**, 2735–2742.
23 A. Braga, S. Gimenez, I. Concina, A. Vomiero and I. Mora-Sero, *J. Phys. Chem. Lett.*, 2011, **2**, 454–460.
24 V. Gonzalez-Pedro, C. Sima, G. Marzari, P. P. Boix, S. Gimenez, Q. Shen, T. Dittrich and I. Mora-Sero, *Phys. Chem. Chem. Phys.*, 2013, **15**, 13835–13843.
25 Z. B. Huang, X. P. Zou and H. Q. Zhou, *Mater. Lett.*, 2013, **95**, 139–141.
26 J. W. Lee, J. D. Hong and N. G. Park, *Chem. Commun.*, 2013, **49**, 6448–6450.
27 J. W. Lee, D. Y. Son, T. K. Ahn, H. W. Shin, I. Y. Kim, S. J. Hwang, M. J. Ko, S. Sul, H. Han and N. G. Park, *Sci. Rep.*, 2013, **3**, 1050.
28 A. Loiudice, A. Rizzo, G. Grancini, M. Biasiucci, M. R. Belviso, M. Corricelli, M. L. Curri, M. Striccoli, A. Agostiano, P. D. Cozzoli, A. Petrozza, G. Lanzani and G. Gigli, *Energy Environ. Sci.*, 2013, **6**, 1565–1572.
29 L. Etgar, D. Yanover, R. K. Capek, R. Vaxenburg, Z. S. Xue, B. Liu, M. K. Nazeeruddin, E. Lifshitz and M. Gratzel, *Adv. Funct. Mater.*, 2013, **23**, 2736–2741.
30 J. Burschka, N. Pellet, S.-J. Moon, R. Humphry-Baker, P. Gao, M. K. Nazeeruddin and M. Gratzel, *Nature*, 2013, **499**, 316–319.
31 G. K. Mor, K. Shankar, M. Paulose, O. K. Varghese and C. A. Grimes, *Nano Lett.*, 2006, **6**, 215–218.
32 T. Stergiopoulos, A. Ghicov, V. Likodimos, D. S. Tsoukleris, J. Kunze, P. Schmuki and P. Falaras, *Nanotechnology*, 2008, **19**, 235602.
33 K. Shankar, G. K. Mor, H. E. Prakasam, O. K. Varghese and C. A. Grimes, *Langmuir*, 2007, **23**, 12445–12449.
34 K. Zhu, N. R. Neale, A. Miedaner and A. J. Frank, *Nano Lett.*, 2007, **7**, 69–74.
35 G. K. Mor, K. Shankar, M. Paulose, O. K. Varghese and C. A. Grimes, *Nano Lett.*, 2005, **5**, 191–195.
36 C. Richter and C. A. Schmuttenmaer, *Nat. Nanotechnol.*, 2010, **5**, 769–772.
37 H. Liu, L. Tao and W. Z. Shen, *Nanotechnology*, 2011, **22**, 155603.
38 X. Y. Yu, B. X. Lei, D. B. Kuang and C. Y. Su, *Chem. Sci.*, 2011, **2**, 1396–1400.
39 L. Tao, Y. Xiong, H. Liu and W. Z. Shen, *J. Mater. Chem.*, 2012, **22**, 7863–7870.
40 M. A. Hines and G. D. Scholes, *Adv. Mater.*, 2003, **15**, 1844–1849.
41 B. R. Hyun, Y. W. Zhong, A. C. Bartnik, L. F. Sun, H. D. Abruna, F. W. Wise, J. D. Goodreau, J. R. Matthews, T. M. Leslie and N. F. Borrelli, *ACS Nano*, 2008, **2**, 2206–2212.
42 W. A. Su and W. Z. Shen, *Solid State Commun.*, 2012, **152**, 798–801.
43 K. Zhu, T. B. Vinzant, N. R. Neale and A. J. Frank, *Nano Lett.*, 2007, **7**, 3739–3746.
44 J. R. Jennings, A. Ghicov, L. M. Peter, P. Schmuki and A. B. Walker, *J. Am. Chem. Soc.*, 2008, **130**, 13364–13372.
45 S. C. Lin, Y. L. Lee, C. H. Chang, Y. J. Shen and Y. M. Yang, *Appl. Phys. Lett.*, 2007, **90**, 143517.
46 Y. L. Lee, B. M. Huang and H. T. Chien, *Chem. Mater.*, 2008, **20**, 6903–6905.
47 D. Zhou, M. Lin, Z. L. Chen, H. Z. Sun, H. Zhang, H. C. Sun and B. Yang, *Chem. Mater.*, 2011, **23**, 4857–4862.
48 H. McDaniel, N. Fuke, J. M. Pietryga and V. I. Klimov, *J. Phys. Chem. Lett.*, 2013, **4**, 355–361.

